X-ray Damage in Protein−Metal Hybrid Structures: A Photoemission Electron Microscopy Study

A. Kade,*,†,‡ K. Kummer,† D. V. Vyalikh,† S. Danzenbächer,† A. Blüher,§ M. Mertig,§ A. Lanzara,∥,⊥ A. Scholl,# A. Doran,# and Serguei L. Molodtsov†

Institute of Solid State Physics, Technische Universität Dresden, 01062 Dresden, Germany, Institute of Air Handling and Refrigeration Dresden, 01309 Dresden, Germany, BioNanotechnology and Structure Formation Group, Max Bergmann Center of Biomaterials and Institute of Materials Science, Technische Universität Dresden, 01062 Dresden, Germany, Department of Physics, University of California, Berkeley, California 94720, Materials Sciences Division, Lawrence Berkeley National Laboratory, Berkeley, California 94720, and Advanced Light Source, Lawrence Berkeley National Laboratory, Berkeley, California 94720

Received: May 4, 2010

Bacterial surface layer protein sheets (S layer) coated with an ultrathin cobalt or silver film were studied by means of laterally resolved near-edge X-ray absorption fine structure spectroscopy performed by photoemission electron microscopy. Comparison with results obtained on pristine S layers allowed us to characterize both chemical interaction and X-ray damage in these protein−metal hybrid systems. In particular, we found that besides direct damage upon exposure to X-ray radiation the biomolecules experience additional contribution of the deposited metals, by low-energy electron generation in the metal particles.

Introduction

Advanced miniaturization of any new generation of electronics reaches the time when established fabrication techniques will meet their limits. Therefore, much current effort is put in the development of novel, unconventional approaches which can open the pathways to new dimensions of structural density. At that, the fabrication of hybrid nanostructures based on biological templates has attracted high attention.[1,2] The unique self-assembly capabilities of biomolecules, such as DNA or bacterial surface protein layers (S layers), have allowed for hybrid nanostructures of extremely small size and with novel material properties.[3−18] Those properties, involving magnetic and transport phenomena as well as chemical interactions, are governed by the electronic structure of such hybrid nanostructures and their inherent constituents. An accordingly large part of the research is currently aimed at the unraveling of the electronic structure of biomolecules and derivative hybrid systems. Given the current attempts in material science to integrate biomolecules into electronic circuits,[19,20] use them as templates to grow metal nanostructures or wire them with metal electrodes,[19−25] the electronic structure of such metal−biomolecule hybrid systems will certainly attract even more attention in the near future. Surely, soft X-ray spectroscopies will be one of the experimental means of choice for that since they have already been proven to grant detailed and diverse insight into biomolecular systems in the past.

Photoemission (PE) and near-edge X-ray absorption fine structure (NEXAFS) spectroscopy provide direct access to occupied and unoccupied electronic states, i.e., the electronic structure, of such systems. Recently, their application allowed us to give a comprehensive characterization of the regular bacterial surface protein layer of *Bacillus sphaericus* NCTC 9602,[26−29] which is widely employed as a template for bottom-up fabrication of hybrid nanostructures. However, without a doubt their meaningful application requires a profound knowledge of their drawbacks including X-ray damage effects. Both experimental techniques require irradiation with sufficiently intense X-ray light, which can come along with notable sample degradation effects, especially in the case of fragile, biological structures.[30−32] A full understanding and characterization of the latter is needed, to estimate their impact on obtained experimental results. Recently, we reported on radiation-induced damage effects for the pristine S layer in detail. In particular, critical doses for the protein layer degradation were obtained for the relevant absorption thresholds of C, N, and O 1s excitations, respectively.[32]

Naturally, after deposition of metal onto biomolecular templates, the resulting hybrid nanostructures can exhibit properties very different from those of the original template. Depending, among others, on their chemical reactivity, interaction between metal particles and the biomolecular template can reach a considerable extent, leading to substantial modifications in the electronic structure and, probably, the X-ray damage behavior, too. While the former has already been studied for a number of metal−biomolecule combinations,[2,33] the latter is widely unknown.

Here we report on a comparative X-ray photoemission electron microscopy (PEEM) study of the S layer of *B. sphaericus* NCTC 9602 before and after deposition of silver and cobalt nanoparticles, respectively. Besides the chemical interaction between the S layer and the two different metals, particular focus was drawn to the question how X-ray-irradiation-induced damage in the hybrid structures differs from that observed for the pristine S layer. Typically, the S layer sheets do not exceed a few square micrometers in size and cover only 80−90% of the substrate surface.[27] The PEEM technique

* To whom correspondence should be addressed. E-mail: andreas.kade@ilkdresden.de.
† Institute of Solid State Physics, Technische Universität Dresden.
‡ Institute of Air Handling and Refrigeration Dresden.
§ Max Bergmann Center of Biomaterials and Institute of Materials Science, Technische Universität Dresden.
∥ Department of Physics, University of California Berkeley.
⊥ Materials Sciences Division, Lawrence Berkeley National Laboratory.
Advanced Light Source, Lawrence Berkeley National Laboratory.

10.1021/jp1040585
Published on Web 06/02/2010

enabled us to perform the spectroscopic studies laterally resolved on single S layer sheets. Thus, interfering contributions from uncovered Si substrate areas are discarded, which makes the interpretation of the measured spectra (considerably) easier.

Experimental Details

Sample Preparation. The S layer was isolated from the bacterium *B. sphaericus* NCTC 9602 and deposited onto naturally oxidized Si wafers [SiO_x/Si(100), n-type, commercial grade]. The detailed protocol for substrate cleaning and S layer deposition was given elsewhere.[32] Scanning electron microscopy revealed a homogeneous surface protein coverage between 80 and 90%. Protein−metal hybrid systems were achieved by deposition of 4 Å Ag or Co onto the pristine S layer using electron beam evaporation at a constant rate of ∼1 Å min^{-1}. The amount of deposited Ag and Co was monitored with a quartz microbalance. To disentangle the effect of direct X-ray damage and potential damage effects by low-energy electrons, we selected cobalt metal with no excitation threshold close to the energy range from the C 1s to O 1s excitation threshold and silver with a high excitation cross section 3d threshold which lies right in-between the C 1s and O 1s edge, close to the N 1s edge.

It has been observed repeatedly that metals tend to structure themselves in a regular cluster array directed by the particular structure of the S layer template.[10,18,34] The pristine and metalized S layer sheets were additionally characterized by transmission electron microscopy (TEM). The observed morphology was found to be in agreement with results of former studies.[18,32]

X-ray Photoemission Electron Microscopy. The experiments were conducted at Advanced Light Source (ALS, Berkeley) using the X-ray photoemission electron microscope (PEEM-2, operating in total electron yield mode) located at the bending-magnet beamline 7.3.1.1. The beamline covers the photon energy range of 200−1300 eV at a spectral resolving power between 1000 and 2000 which is sufficient for most imaging investigations. For radiation monochromatization, the beamline is equipped with a spherical-grating monochromator. In the considered photon energy range of C 1s, N 1s, and O 1s excitations, a low line-density grating (200 lines/mm) was utilized. A Ti filter was employed to eliminate higher-order light for the C 1s and N 1s measurements. It was not used during the O 1s experiments. The flux density was mostly reduced by aperturing the beam upstream of the monochromator. By these arrangements, the photon-flux density during S-layer irradiation, which was calibrated with the photodiode, was typically decreased to approximately 10^{13} photons/(s cm^2) for C 1s and N 1s and 10^{14} photons/(s cm^2) for the O 1s measurements. As found in the experiments, this flux-density value exhibits a good compromise between the experimental statistics and the level of the sample damage. To reduce the irradiated area in the experiments, an extraordinary small exit aperture of 100 μm was employed. The beam spot at the sample surface was 35 × 100 μm^2.

The PEEM micrograph patterns were taken with an electrostatic optical system as described previously.[32] Thereby, a lateral resolution of ∼50 nm was achieved. By recording signals sequentially with an incrementally increasing photon energy, NEXAFS microspectra for each imaging point of the CCD camera (1 pixel ∼ 33 nm) were acquired. An example PEEM image taken at 283 eV photon energy is shown in Figure 1. Light colors represent uncovered substrate areas which give high signal intensity, whereas S layer covered regions appear as dark areas. There are basically two discrete levels of recorded PEEM intensity which suggests relative homogeneity of the deposited S layer. Since skin irradiation doses were significantly reduced, the statistics of each individual one-pixel measurement was not enough to derive reliable conclusions on the line shape of the underlying NEXAFS spectrum. Therefore, the signals were integrated over several dark areas.

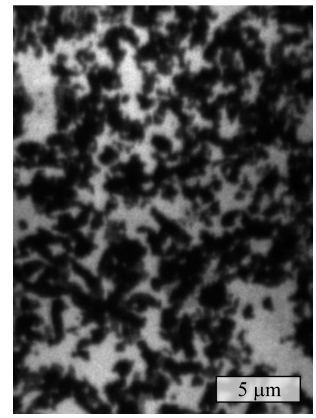

Figure 1. PEEM micrograph taken at 283 eV photon energy. Dark areas with low electron yield represent the S layer sheets, light areas uncovered parts of the substrate. The NEXAFS spectra were extracted by summation over multiple dark areas.

The measured NEXAFS spectra were normalized to the incident photon flux using each time a clean gold reference sample calibrated with an X-ray photodiode (IRD, model AXUV-100). For presentation, the spectra were additionally rescaled such that they coincide in the pre-edge and in the σ^* range beyond the absorption edge which eases the identification of relative changes between different spectra.

Results

Chemical Interaction. The characteristic chemical structure common to all proteins is the peptide bond. Various comprehensive studies have addressed the role of this structure for the X-ray absorption properties of proteins. In particular, it has been established that the presence of peptide bonds gives rise to a sharp π^* resonance in the NEXAFS of the C, N, and O 1s absorption edge at 288.1, 401.2, and 531.8 eV excitation energy, respectively. These resonances are highly sensitive to any alteration of the peptide unit. A clear loss in intensity has been observed when proteins undergo, for instance, X-ray damage or chemical modification.[35]

Thus, monitoring these distinct π^* peaks in protein NEXAFS spectra ($\pi^*_{peptide}$) allowed us to effectively probe the chemical interaction between the peptide units and deposited metals. In Figure 2, we show the C, N, and O 1s NEXAFS spectra for the pristine S layer together with the spectra which were obtained after deposition of 4 Å cobalt and silver, respectively. The spectra taken on pristine S layer sheets (solid lines) feature sharp, distinct 1s → $\pi^*_{peptide}$ resonances at 288.1, 401.2, and 531.8 eV, which reflect transitions from the respective core levels into the peptide orbital of π^* symmetry. In the C 1s NEXAFS spectrum, an additional π^* peak shows up at 285 eV which is due to excitations of aromatic structures in the protein side chains.[28,29,36] These spectral shapes are similar to those reported before for proteins in general[37−39] and the S layer in particular.[26,28,29] Hereafter, we take them as the spectral fingerprint of pristine, undamaged S layer sheets.

Upon metal deposition, notable modifications in the spectra are observed. Most obviously, the $\pi^*_{peptide}$ resonances experience a loss in intensity at all three absorption edges. At that, the loss

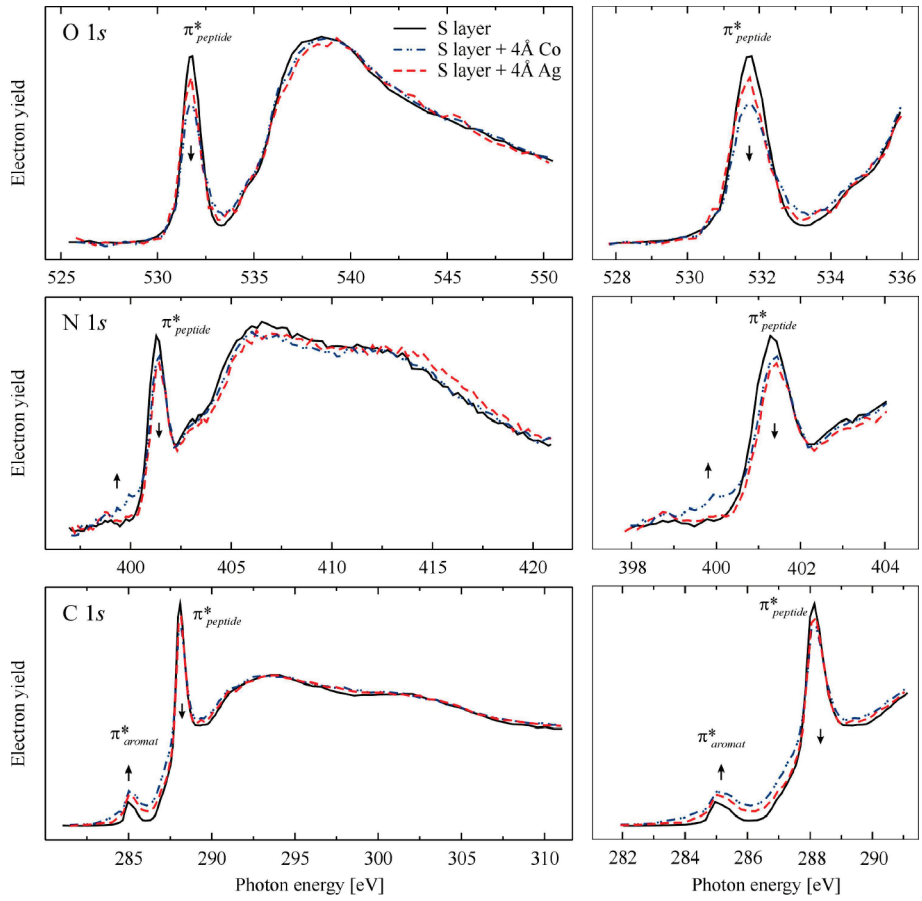

Figure 2. (left) NEXAFS spectra of the protein layer before and after deposition of 4 Å Co and Ag, respectively. After metal deposition, a notable loss in intensity of the sharp $\pi^*_{peptide}$ peaks at 288.1, 401.3, and 531.8 eV is observed at the C 1s, N 1s, and O 1s absorption edge, respectively, which is due to chemical interaction. (right) Magnification of the respective π^* regions.

is generally more pronounced after deposition of 4 Å cobalt (dashed-dotted lines) than after silver deposition (dashed lines). However, the general shape of the S layer spectra is conserved. In particular, the $\pi^*_{peptide}$ resonances still appear as distinct, sharp peaks, apart from the intensity loss. This indicates that the S layer remains in large part unaffected by the metal deposition. On the other hand, the $\pi^*_{peptide}$ intensity loss clearly shows that the metal deposition induces modifications of the peptide bonds in minor parts of the S layer, possibly its outward regions in immediate contact with the metals. These modifications seem in general more severe in the case of cobalt than in the case of silver deposition, which is consistent with the lower reactivity of the noble metal.[40] In the C 1s spectrum, the decline in $\pi^*_{peptide}$ intensity after metal deposition comes along with signal enhancement in the region around 285 eV. This has been previously interpreted as an effect of peptide unit damage and subsequent rearrangement of loose carbon atoms into carbon−carbon networks.[32] Again, the effect is stronger after cobalt than after silver deposition. Furthermore, in the former case, and less pronounced in the latter case, too, additional excitations are observed in N 1s NEXAFS which lie below the intense $\pi^*_{peptide}$ peak in energy, i.e., at ~398 − 400 eV. They are most likely due to newly forming carbon−nitride compounds between loose C and N atoms.[32,41]

In summary, the spectra reveal only moderate modification of the S layer upon chemical interaction with the deposited silver or cobalt material. Although the characteristic $\pi^*_{peptide}$ resonances lose some intensity, the spectral shape observed for the pristine S layer is principally conserved. Accordingly, we assume that moderate protein−metal interaction, that is slightly higher for cobalt than for silver deposition, involves only minor parts of the S layer sheets, whereas the main part of the protein structure remains unaffected.

X-ray Radiation Damage. Having characterized the chemical interaction in the protein−metal hybrid systems, we will now turn to the important issue of their X-ray damage behavior. To this end, a brief description of the X-ray damage effects in the pristine S layer will be given, which will then be compared with effects observed for the hybrid structures.

The photon flux at the PEEM beamline, we used in Berkeley, exceeds that applied for our spectroscopic S layer studies at BESSY (Berlin)[42] by at least a factor 10^2. In consequence, X-ray damage reaches a considerable extent and induces rapid damage-derived changes in the NEXAFS spectra already within short periods of irradiation. Figure 3 shows the relative spectral evolution during the first 10 scans of the C, N, and O 1s NEXAFS of pristine S layer sheets. The spectra are normalized like described previously.

At the O 1s edge, a considerable scan-by-scan decline of the $\pi^*_{peptide}$ intensity is observed. Accordingly, a large number of peptide bonds must undergo severe radiation damage. At the same time, a strong absolute decrease in O 1s intensity (not visible due to normalization) points to surface desorption of oxygen atoms, released from broken peptide bonds.[32,43] Note that there is also a notable shift and broadening of the O 1s → π^* line shape toward lower excitation energy. We assume that it reflects incipient contributions from the SiO_x substrate which are due to desorption of overlying protein material. Spectra taken on uncovered substrate areas feature a rather broad structure in the π^* region with the peak maximum at 531.2 eV (not shown).

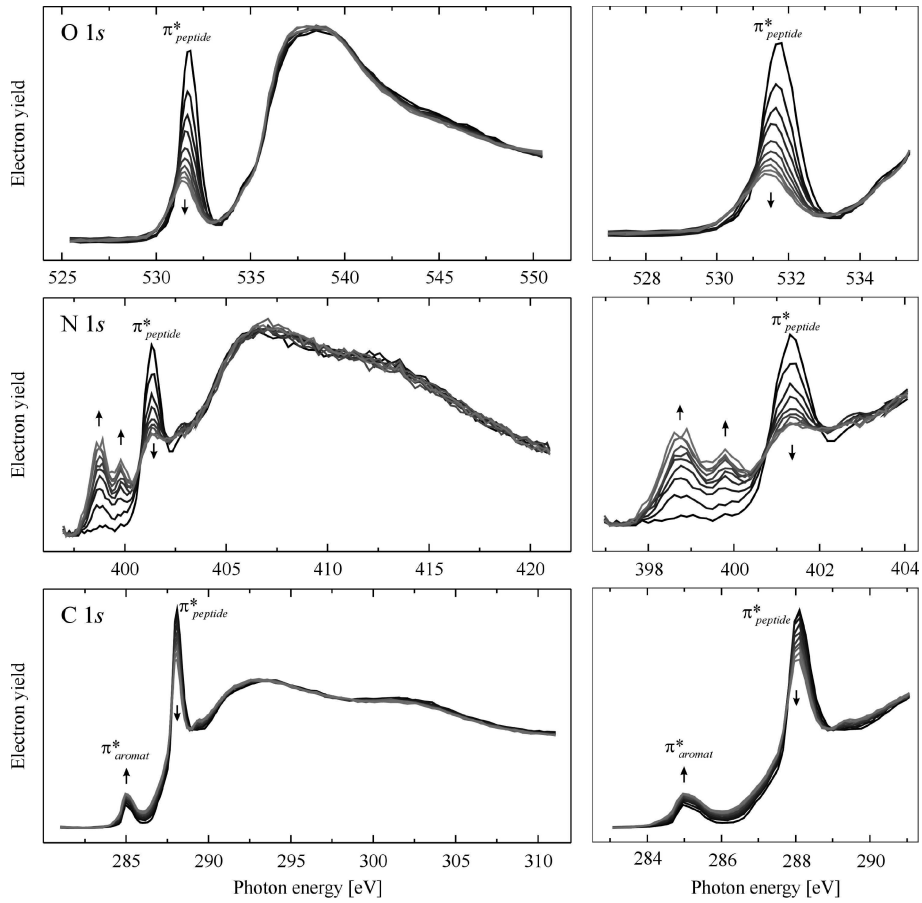

Figure 3. (left) Spectral changes in the C, N, and O 1s NEXAFS of pristine S layer sheets during the first 10 scans. (right) Magnification of the respective π^* regions.

Its overlap with the π^*_{peptide} resonance would result in a broadening and energy shift of the π^* shape similar to what has been observed in Figure 3. Since no further structures show up in the π^* and σ^* region, we suppose that no additional type of oxide forms at the surface.

The π^*_{peptide} peak at the N 1s edge exhibits a similarly rapid loss in intensity. At the same time, an additional two-peak structure emerges at ∼398−400 eV. In our previous study,[32] it was attributed to newly forming carbon−nitride compounds. The only slight loss in total N 1s intensity proposes that most of the released nitrogen atoms are incorporated in these compounds rather than desorbed from the surface. Changes in the C 1s NEXAFS are comparatively small. Besides loss in π^*_{peptide} signal, there is some intensity enhancement in the region around 285 eV excitation energy at no decrease in absolute C 1s absorption. This is consistent with a previously proposed scenario where loose carbon atoms from disintegrated peptide bonds do not desorb but build carbon−carbon networks, possibly involving amorphous or carbidic carbon.[32]

The generally more pronounced damage effects in the N 1s and O 1s photon energy range are caused by the increase in typical exposure dose from ∼3 to ∼13 to ∼17 MGy per scan when going from the C 1s to N 1s to O 1s edge.[32] We gave a more comprehensive discussion of the observed X-ray radiation-induced damage of pristine S layer sheets, including critical doses, elsewhere.[32] Here, we will now concentrate on the relative changes in X-ray damage behavior after deposition of silver and cobalt.

To this end, we compare the spectral evolution in the π^* region of each of the three relevant absorption edges for both pristine and metalized S layer sheets. In particular, changes in the relative decrease of the π^*_{peptide} peak intensity give a good estimate of the extent of X-ray damage in both cases. To deduct the slight intensity losses upon metal deposition, the measured spectra were rescaled such that π^*_{peptide} intensities coincide after metal deposition again, i.e., in the "first scan" spectra. In doing so, one can compare their radiation-damage-induced relative decline directly in the spectra. This is shown in Figure 4.

Dashed horizontal lines mark the relative π^*_{peptide} peak intensity after 1, 5, and 10 scans in the N and O 1s NEXAFS spectra and after 1, 5, and 7 scans in the C 1s spectra. Most strikingly, in all three energy windows, the decrease of the π^*_{peptide} signal is strongest for the pristine S layer. Both the silver and the cobalt metalized protein layers show an, in general, much slower rate of peptide bond disintegration. However, there are also evident differences between the two metals. In the energy range of N and O 1s excitations, the cobalt-metalized layer seems considerably more stable, whereas the silver−protein structure exhibits a rapid damage rate which in the case of the O 1s edge almost reaches that of the pristine S layer. Accordingly, it shows a similar broadening and shift of the π^* resonance due to massive protein desorption and thus incipient substrate contributions. In the C 1s range, differences are not that drastic. There, however, the silver metalization seems to breed the most stable system.

Despite quantitative differences, the qualitative spectral changes appear to be similar for both the pristine and metalized S layer. More precisely, besides the general decrease of the π^*_{peptide} absorption, we observed the same tiny enhancement in C 1s absorption around 285 eV as well as the rise of a two-peak structure at 398−400 eV in the N 1s spectra in all three

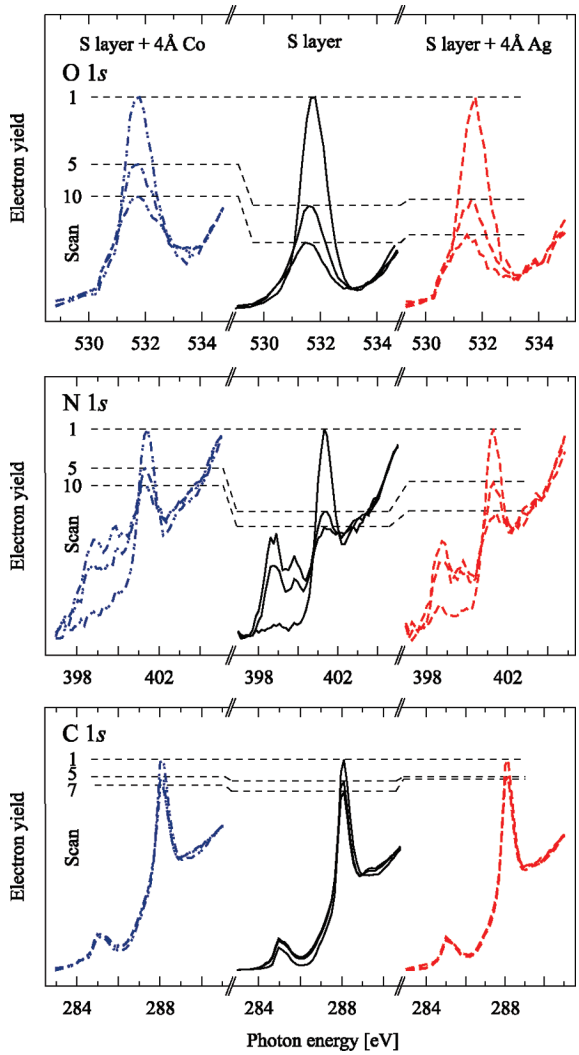

Figure 4. X-ray irradiation-induced evolution of the C, N, and O 1s NEXAFS spectra of pristine and metalized S layer sheets. The dashed horizontal lines mark the relative intensity of the $\pi^*_{peptide}$ peak after the given number of scans, which represents a measure of X-ray damage. It exhibits the most rapid decline for the pristine S layer, regardless of the excitation edge. At higher photon energies of N and O 1s excitations, the damage is weaker by far in the case of cobalt metalization, whereas at photon energies in the C 1s range silver metalization slows down peptide bond disintegration the most.

systems. As in the case of the pristine S layer, there were also no notable evolutions in the σ^* regions of the NEXAFS spectra for the protein−metal hybrid systems. This suggests that carbon and nitrogen atoms which are released during peptide bond breaking form similar types of carbon−carbon and carbon−nitride compounds in pristine and metalized S layers and do not undergo massive chemical interaction with metal particles.

Discussion

Summarizing the obtained results, the qualitative X-ray damage behavior of the S layer appears to be unaffected by the deposition of silver or cobalt metal, but the rate of disintegration of the protein structure seems to be considerably altered, at similar absolute X-ray exposure. In the following, we address possible reasons for this difference between the pristine protein layer and protein−metal hybrid structures. We also discuss why, depending on the chosen photon energy range, such a large difference even between the two deposited metals is obsereved.

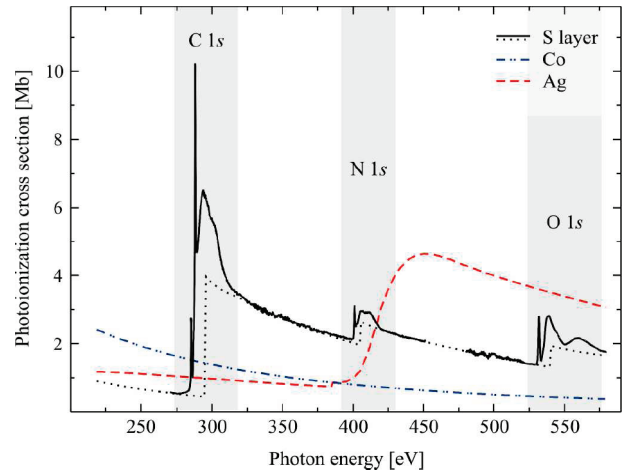

Figure 5. Calculated total atomic photoionization cross sections of silver and cobalt together with the spectral dependence of X-ray absorption by the pristine S layer.

In our mind, metal deposition can come along with two principal effects on the X-ray damage behavior of the protein layer: (i) attenuation of effective incident photon intensity reaching the S layer due to absorption by the covering metal and (ii) additional, collateral contribution of the deposited metals to X-ray damage of the S layer. More precisely, absorption of X-ray photons by the metal leads to emission of Auger or photoelectrons which easily lose their kinetic energy by inelastic scattering because of the high density of valence states in the metal. These low kinetic energy electrons can deeply penetrate the S layer because of their relatively large electron mean free path[44] and are known to be a main driving force in damage of biomolecules.[45,46] The processes, (i) and (ii), have opposite trends to affect the damage rate. On one hand, high absorption in the metal leads to less effective X-ray exposure of the S layer and thus less direct damage. On the other hand, it also results in generation of low-energy electrons in the metal and thus higher collateral damage.

Since we always observed lowered decay rates for the metalized layers, we believe that the former process, i.e., X-ray attenuation by absorption by the metal, is dominant. However, our data also suggest a severe contribution to protein damage by low-energy electrons originating from the metal. Looking at the atomic photoionization cross sections for silver and cobalt,[47] which are plotted in Figure 5, there is a close correlation between electron generation in the metals and observed damage of the S layer.

In the O 1s photon energy range, for instance, the photoionization cross section is significantly higher for silver than for cobalt. This comes along with a considerably faster disintegration of peptide bonds in the silver−protein structure almost comparable to the rate for the pristine S layer (cf. Figure 4). To a lower extent, the same holds for the N 1s photon energy range where massive excitation of Ag 3d electrons only sets in. The situation is opposite in the case of the C 1s energy range. Here both Ag and Co photoionization cross sections are comparable, with the latter being only a little higher. Again, this correlates with the observed protein damage rate which is slightly higher for cobalt but basically on the same level for both metals.

In summary, X-ray damage in the protein−metal hybrid structures seems to be driven by the two processes. The first is direct damage upon massive X-ray exposure, as observed for the pristine S layer, too. The deposited metal, however, absorbs part of the incident photon flux and, thus, partly screens the

protein layer from irradiation. In consequence, the latter experiences less direct damage in the hybrid than in the pristine state when exposed to similar absolute doses. The second is collateral damage by low-energy electrons generated in the deposited metals. These processes reveal antagonistic trends, but for the silver and cobalt metalized S layer we found the former process to be dominant. However, in the case of high photoionization cross section of the metal, collateral X-ray damage almost neutralizes its radiation screening effect, as observed in the case of silver in the O 1s energy range.

Conclusions

We performed X-ray PEEM studies on pristine S layer sheets and after deposition of 4 Å cobalt or of 4 Å silver, respectively. At that, the lateral resolution enabled us to avoid undesired contributions from uncovered substrate areas. In doing so, we were able to obtain undisturbed NEXAFS spectra from both pristine and metalized S layer sheets. The π^*_{peptide} resonance at the three relevant absorption edges, i.e., C, N, and O 1s, was exploited as a probe for both protein−metal interaction and X-ray radiation-induced damage. It was found that metal deposition leaves the protein layer in large part unaffected, though, especially in the case of the more reactive cobalt, notable changes with respect to the pristine protein structure were detected.

X-ray radiation-induced damage left qualitatively the same spectral fingerprints for both pristine and hybrid S layers. However, upon metal deposition, the disintegration of peptide bonds was significantly lowered, which we explained by attenuation of the effective dose acting on the protein layer. Besides direct X-ray damage, which has also been observed for pristine S layers, metalization seems to open an additional channel of indirect, well-known protein damage by low-energy electrons generated in the deposited metal.

Usually, we found attenuation of the effective dose by the metal overlayer the dominating process. But since, depending on the deposited metal and the applied photon energies, the additional damage can reach a comparable level, it must be accounted for in any spectroscopic study of protein−metal hybrid systems, in particular, and biomolecule−metal complexes, in general, where critical doses of X-ray exposure are involved.

Acknowledgment. We would like to thank Beate Katzschner for the preparation of the S layer sheets. This work was financially supported by the DFG (Grant Nos. MO 1049/5-1, LA 655/10-4, and ME 1256/13-1).

References and Notes

(1) Mann, S. *Nature* **1993**, *365*, 499.
(2) Katz, E.; Willner, I. *Angew. Chem., Int. Ed.* **2004**, *43*, 6042.
(3) McMillan, R. A.; Paavola, C. D.; Howard, J.; Chan, S. L.; Zaluzec, N. J.; Trent, J. D. *Nat. Mater.* **2002**, *1*, 247.
(4) Mertig, M.; Colombi, Ciacchi, L.; Seidel, R.; Pompe, W.; De Vita, A. *Nano Lett.* **2002**, *2*, 841.
(5) Seidel, R.; Colombi, Ciacchi, L.; Weigel, M.; Pompe, W.; Mertig, M. *J. Phys. Chem. B* **2004**, *108*, 10801.
(6) Queitsch, U.; Mohn, E.; Schäffel, F.; Schultz, L.; Rellinghaus, B.; Blüher, A.; Mertig, M. *Appl. Phys. Lett.* **2007**, *90*, 113114.
(7) Györvary, E.; O'Riordan, A.; Quinn, A.; Redmond, G.; Pum, D.; Sleytr, U. B. *Nano Lett.* **2003**, *3*, 315.
(8) Douglas, K.; Clark, N. A.; Rothschild, K. J. *Appl. Phys. Lett.* **1990**, *56*, 692.
(9) Shenton, W.; Pum, D.; Sleytr, U. B.; Mann, S. *Nature* **1997**, *389*, 585.
(10) Moore, J. T.; Beale, P. D.; Winnigram, T. A.; Douglas, K. *Appl. Phys. Lett.* **1998**, *72*, 1840.
(11) Dieluweit, S.; Pum, D.; Sleytr, U. B. *Supramol. Sci.* **1998**, *5*, 15.
(12) Mertig, M.; Kirsch, R.; Pompe, W.; Engelhardt, E. *Eur. Phys. J. D* **1999**, *9*, 45.
(13) Hall, S. R.; Shenton, W.; Engelhardt, H.; Mann, S. *Chem. Phys. Chem.* **2001**, *3*, 184.
(14) Mertig, M.; Wahl, R.; Lehmann, M.; Simon, R.; Pompe, W. *Eur. Phys. J. D* **2001**, *16*, 317.
(15) Wahl, R.; Mertig, M.; Raff, J.; Selenska-Pobell, S.; Pompe, W. *Adv. Mater.* **2001**, *13*, 736.
(16) Wahl, R.; Engelhardt, H.; Pompe, W.; Mertig, M. *Chem. Mater.* **2005**, *17*, 1887.
(17) Aichmayer, B.; Mertig, M.; Kirchner, A.; Paris, O.; Fratzl, P. *Adv. Mater.* **2006**, *18*, 915.
(18) Pompe, W.; Mertig, M.; Kirsch, R.; Engelhardt, H.; Kronbach, T. *Microreaction Technology*; Springer: Berlin-Heidelberg-New York, 1998; p 104.
(19) Offenhäusser, A.; Rinaldi, R.; Lockwood, D. J. *Nanobioelectronics*; Springer: New York, 2009.
(20) Weibel, N.; Grunder, S.; Mayor, M. *Org. Biomol. Chem.* **2007**, *5*, 2343.
(21) Vu, X. T.; GhoshMoulick, R.; Eschermann, J. F.; Stockmann, R.; Offenhäusser, A.; Ingebrandt, S. *Sens. Actuators. B* **2010**, *144*, 354.
(22) Björk, P.; Herland, A.; Hamedi, M.; Inganäs, O. *J. Mater. Chem.* **2010**, *20*, 2269.
(23) Kretzschmar, I.; Reed, A. M. *Dekker Encyclopedia Nanosci. Nanotechnol.* **2009**, 2.
(24) Liu, Y.; Offenhäusser, A.; Mayer, D. *Biosens. Bioelectron.* **2010**, *25*, 1173.
(25) Willner, I.; Baron, R.; Willner, B. *Biosens. Bioelectron.* **2007**, *22*, 1841.
(26) Vyalikh, D. V.; Danzenbächer, S.; Mertig, M.; Kirchner, A.; Pompe, W.; Dedkov, Yu. S.; Molodtsov, S. L. *Phys. Rev. Lett.* **2004**, *93*, 238103.
(27) Vyalikh, D. V.; Kirchner, A.; Danzenbächer, S.; Dedkov, Yu. S.; Kade, A.; Mertig, M.; Molodtsov, S. L. *J. Phys. Chem. B* **2005**, *109*, 18620.
(28) Vyalikh, D. V.; Kirchner, A.; Kade, A.; Danzenbächer, S.; Dedkov, Yu. S.; Mertig, M.; Molodtsov, S. L. *J. Phys.: Condens. Matter* **2006**, *18*, 131.
(29) Maslyuk, V. V.; Mertig, I.; Bredow, T.; Mertig, M.; Vyalikh, D. V.; Molodtsov, S. L. *Phys. Rev. B* **2008**, *77*, 045419.
(30) Zubavichus, Y.; Zharnikov, M.; Shaporenko, A.; Fuchs, O.; Weinhardt, L.; Heske, C.; Umbach, E.; Denlinger, J. D.; Grunze, M. *J. Phys. Chem. A* **2004**, *108*, 4557.
(31) Kummer, K.; Vyalikh, D. V.; Gavrila, G.; Kade, A.; Weigel-Jech, M.; Mertig, M.; Molodtsov, S. L. *J. Electron Spectrosc. Relat. Phenom.* **2008**, *163*, 59.
(32) Kade, A.; Vyalikh, D. V.; Danzenbächer, S.; Kummer, K.; Blüher, A.; Mertig, M.; Lanzara, A.; Scholl, A.; Doran, A.; Molodtsov, S. L. *J. Phys. Chem. B* **2007**, *111*, 13491.
(33) Compagnon, I.; Tabarin, T.; Antoine, R.; Broyer, M.; Dugourd, P.; Mitric, R.; Petersen, J.; Bonacic-Koutecky, V. *J. Chem. Phys.* **2006**, *125*, 164326.
(34) Panhorst, M.; Brückl, H.; Kiefer, B.; Reiss, G.; Santarius, U.; Guckenberger, R. *J. Vac. Sci. Technol. B* **2001**, *19*, 722.
(35) Wang, J.; Morin, C.; Li, L.; Hitchcock, A. P.; Scholl, A.; Doran, A. *J. Electron Spectrosc. Relat. Phenom.* **2009**, *170*, 25.
(36) Zubavichus, Y.; Shaporenko, A.; Grunze, M.; Zharnikov, M. *J. Phys. Chem. A* **2005**, *109*, 6998.
(37) Gordon, M. L.; Cooper, G.; Morin, C.; Araki, T.; Turci, C. C.; Kaznatcheev, K.; Hitchcock, A. P. *J. Phys. Chem. A* **2003**, *107*, 6144.
(38) Cooper, G.; Gordon, M.; Tulumello, D.; Turci, C.; Kaznatcheev, K.; Hitchcock, A. P. *J. Electron Spectrosc. Relat. Phenom.* **2004**, *137*, 795.
(39) Zubavichus, Y.; Shaporenko, A.; Grunze, M.; Zharnikov, M. *J. Phys. Chem. B* **2008**, *112*, 4478.
(40) Cf. reactivity series of metals.
(41) Shimoyama, I.; Wu, G.; Sekiguchi, T.; Baba, Y. *Phys. Rev. B* **2000**, *62*, R6053.
(42) Molodtsov, S. L.; Fedoseenko, S. I.; Vyalikh, D. V.; Iossifov, I. E.; Follath, R.; Gorovikov, S. A.; Brzhezinskaya, M. M.; Dedkov, Y. S.; Püttner, R.; Schmidt, J.-S.; Adamchuk, V. K.; Gudat, W.; Kaindl, G. *Appl. Phys. A: Mater. Sci. Process.* **2009**, *94*, 501.
(43) Williams, S.; Zhang, X.; Jacobsen, C.; Kirz, J.; Lindaas, S.; van't Hof, J.; Lamm, S. S. *J. Microsc.* **1993**, *170*, 155.
(44) Seah, M. P.; Dench, W. A. *Surf. Interface Anal.* **1979**, *1*, 2.
(45) Sanche, L. *Eur. Phys. J. D* **2005**, *35*, 367.
(46) Barrios, R.; Skurski, P.; Simons, J. *J. Phys. Chem. B* **2002**, *106*, 7991.
(47) Yeh, J. J. *Atomic Calculation of Photoionization Cross-Sections and Asymmetry Parameters*; Gordon and Breach Science Publishers: Langhorne, PE (USA), 1993. Yeh, J. J.; Lindau, I. *At. Data Nuclear Data Tables* **1985**, *32*, 1.

JP1040585